sustainability

MDPI

Article

Ecological Health Assessment of the Yuejiang River in Sichuan Province Based on the PCA–Entropy Weight Method

Diancheng Wang, Wende Chen *, Jiali Zhou, Rui He, Yuhang Hou and Heliang Xu

College of Geography and Planning, Chengdu University of Technology, Chengdu 610059, China
* Correspondence: chenwende@cdut.edu.cn

Abstract

River-health assessment in small rural watersheds requires the integration of multiple environmental indicators, yet correlated variables may be repeatedly represented when they are weighted independently. This study evaluated the ecological health of the Yuejiang River in Dongpo District, Meishan City, Sichuan Province, for 2011, 2018, and 2024 using a principal component analysis (PCA)–entropy weighting framework. Fourteen effective indicators represented riparian habitat, climate–hydrology, water environment, human disturbance, and water quality. Water-quality data for 2011 and 2018 were treated as monitored regional background conditions, whereas continuous reach-scale observations were unavailable for 2024 and scenario-constrained regional background inputs were therefore used. PCA retained four components that explained 95.94% of the total variance, and the resulting combined weights were used to calculate the River Health Index (RHI). Mean RHI values increased from 0.290 in 2011 to 0.578 in 2018 and 0.634 in 2024. In 2024, 83.92% of the mapped assessment area was classified as Good and 16.08% as Moderate. High PCA loadings and combined weights are interpreted as statistical contributions within the assessment framework, rather than as evidence of direct ecological causation. The results support temporal comparison and identification of relatively weak reaches, while the 2024 findings should be interpreted as conditional on the adopted water-quality background scenario.

Keywords: Yuejiang River; PCA–entropy weight method; River Health Index; ecological health; water quality condition

1. Introduction

River-health assessment has progressively shifted from single water-quality evaluation toward an integrated appraisal of ecological structure, habitat condition, hydrology, and human pressure. This transition is particularly relevant to small rural watersheds, where riparian vegetation, agricultural land use, flow conditions, and local pollution pressures can vary markedly over short distances. An appropriate assessment framework for such rivers therefore needs to capture both overall environmental condition and spatially concentrated human disturbance.

Recent river-health studies increasingly integrate physical, chemical, biological, and landscape information in small- and medium-sized or urban rivers [1–4]. Fuzzy and combination-weight approaches have also been used to synthesize heterogeneous indicators [5–7], while assessment systems for strongly disturbed rivers and recent game-theory, cloud-model, and restoration-oriented frameworks have extended this work [8–12]. Despite these advances, weight determination remains sensitive to indicator redundancy. In small

Academic Editor: Agostina Chiavola

Received: 21 July 2026
Revised: 20 August 2026
Accepted: 28 August 2026
Published: 2 September 2026

rural watersheds, FVC and NDVI may describe closely related vegetation information, while several water-quality variables can represent the same regional background. If such variables are weighted independently, overlapping information may be counted more than once.

Entropy weighting objectively reflects variation among observations, but it does not account for correlation among indicators. PCA can identify shared variation and reduce information redundancy, although the reliability of its interpretation depends on the structure and size of the dataset. In this study, PCA was therefore used only as an exploratory auxiliary procedure, rather than as an independent river-health model. The combined procedure uses PCA to diagnose shared information among correlated indicators while retaining the dispersion information quantified by entropy weighting.

Accordingly, this study aimed to (1) compare the ecological health of the Yuejiang River in 2011, 2018, and 2024 using a consistent indicator system and (2) identify relatively weak reaches requiring management attention. Its methodological contribution lies in explicitly using PCA to moderate the repeated representation of correlated indicators before entropy-based combined weighting. The framework integrates riparian vegetation, landscape pattern, hydrology, water quality, and human disturbance using data types that are generally obtainable for small rural watersheds.

2. Materials and Methods

The overall analytical workflow, including data preprocessing, indicator screening, correlation analysis, principal component analysis, entropy weighting, combined weighting, RHI calculation, and ecological consistency analysis, is shown in Figure 1.

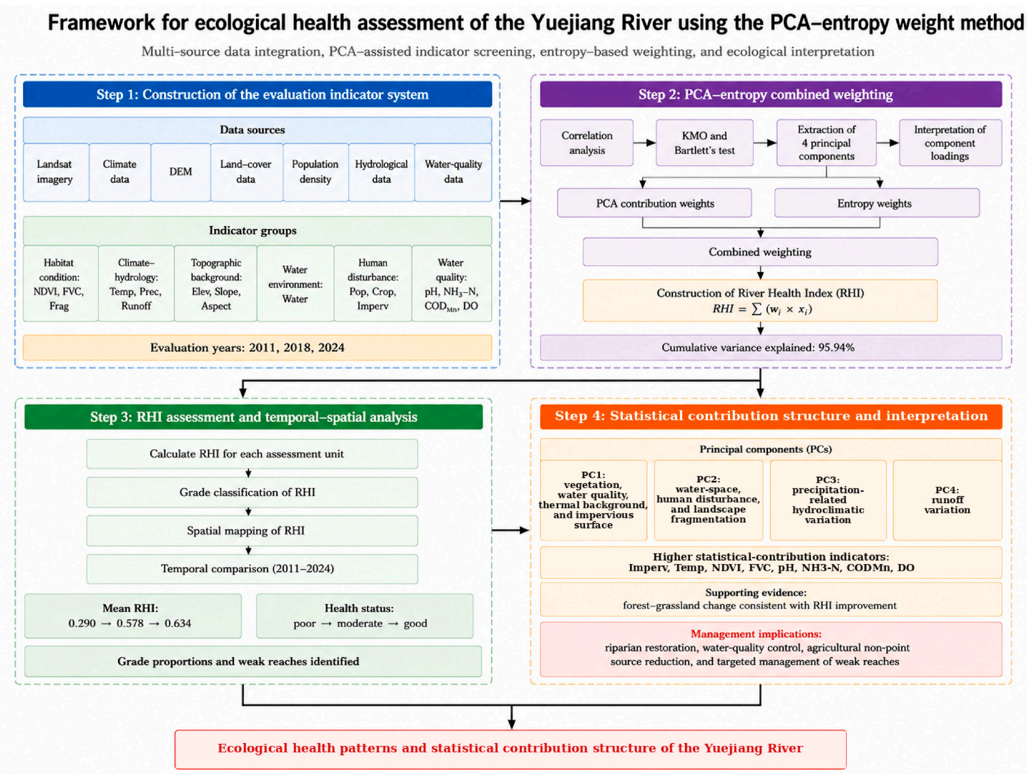

Figure 1. Technical flowchart.

2.1. Study Area

The Yuejiang River is located in central Sichuan Province (103°41′–104°01′ E, 30°00′–30°09′ N) (Figure 2) and belongs to the Minjiang River system. The study reach is situated in Dongpo District, Meishan City, within the transition between the Chengdu Plain and the hilly region of central Sichuan. It has a total length of approximately 7.89 km and a study area of 35.98 hm^2.

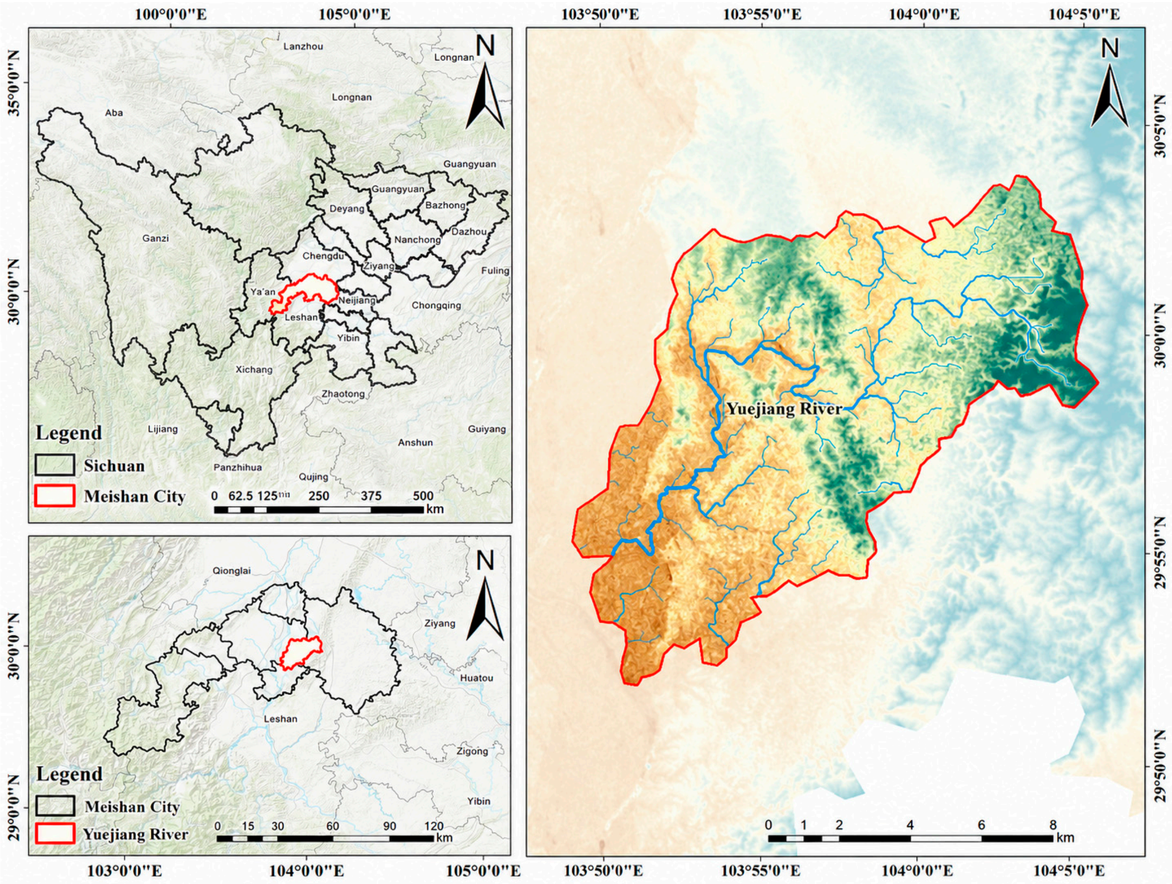

Figure 2. Location and study area of the Yuejiang River.

The study area is dominated by plains and terraces, with elevations ranging from 392 to 535 m. Topography generally declines from northwest to southeast, and influences runoff generation and flow accumulation. The region has a subtropical humid monsoon climate. Based on the meteorological data used in this study, annual mean temperature ranged from 17.23 to 18.25 °C and annual precipitation from 1129.8 to 1653.1 mm during 2011–2024. Rainfall is strongly seasonal, with concentrated summer precipitation contributing to short-term variation in river and riparian conditions.

2.2. Data Sources

The assessment years 2011, 2018, and 2024 were selected primarily on the basis of the availability and comparability of the multisource datasets required for the analysis. They represent early, intermediate, and recent conditions within the study period, and are not intended to define the boundaries of a specific restoration project. The datasets included remote-sensing, meteorological, hydrological, land-use, water-quality, and socioeconomic information (Table 1). All spatial datasets were projected to a common coordinate system, clipped and registered to the study area, and summarized within the predefined riparian buffer and six assessment units.

Remote-sensing data were obtained from Landsat imagery and were used to derive the normalized difference vegetation index (NDVI) and fractional vegetation cover (FVC) [13]. Meteorological variables, including annual precipitation and mean temperature, were obtained from the China Meteorological Administration and corresponding gridded climate datasets [14]. Digital elevation model (DEM) data were used to derive elevation, slope, and aspect. Land-use data were used to calculate water area ratio, riverbank farmland proportion, landscape fragmentation, and riverbank construction-land proportion [15,16]. Population density [17] data were used to characterize human disturbance, while impervious-surface information was used to further represent anthropogenic land-use intensity. Annual mean runoff was obtained from the Sichuan Water Resources Bulletin, Meishan Water Resources Bulletin, and relevant hydrological statistics, and was matched to the six assessment units according to river-section location and hydrological connectivity.

Water-quality indicators included pH, NH_3-N, CODMn, and DO. Historical observations for 2011 and 2018 were obtained from the long-term national surface-water quality dataset compiled by Lin et al. [18]. The Leshan Minjiangdajiao monitoring station (MonitoringLocationIdentifier = 49) was selected as the regional background station because it belongs to the same Minjiang River system and provides complete records for the four indicators. For 2011 and 2018, all available observations of pH, NH_3-N, CODMn, and DO within each calendar year were summarized as annual means and assigned uniformly to the six assessment units as common year-specific regional background values; no spatial interpolation from the station to individual Yuejiang River reaches was performed. For 2024, continuous reach-scale monitoring records for the six assessment units were also unavailable. The July 2024 Meishan Surface-Water Quality Monthly Report (released on 17 July 2024) and the 2024 Meishan Ecological Environment Status Bulletin (released on 27 June 2025) were therefore used only to characterize and check the regional water-quality context [19,20]. These official reports were not used as direct numerical sources for the six assessment units. The numerical 2024 inputs were predefined scenario-constrained regional background estimates anchored to the monitored 2018 annual background. Limited differences among the six unit inputs were introduced only within this predefined scenario to distinguish the mainstream and tributary and the upper, middle, and lower reaches. No station-to-reach interpolation, monitoring-based reach assignment, or claim of observed reach-scale gradients was made. Accordingly, the 2024 water-quality values are conditional scenario inputs rather than measured reach-scale concentrations, and are used mainly to support comparison among the three assessment periods.

For transparency and reproducibility, the exact water-quality inputs used for the six assessment units in 2011, 2018, and 2024, together with their data status and assignment basis, are reported in Supplementary Table S2. The 2024 values listed there are scenario inputs, rather than observed reach-scale concentrations.

Before PCA and entropy weighting, all retained indicators were transformed to a common 0–1 scale according to their ecological direction. For positive indicators, larger standardized values represented more favorable conditions within the observed range; negative indicators were transformed in the opposite direction. The resulting standardized indicators were then used consistently across the six assessment units to calculate the River Health Index (RHI).

Statistical analyses, including correlation analysis, KMO and Bartlett's tests, and PCA, were conducted using IBM SPSS Statistics 27.0 (IBM Corp., Armonk, NY, USA).

Table 1. Datasets, sources, spatial resolution/statistical units, and preprocessing methods.

Indicator	Dataset	Spatial Resolution/ Statistical Unit	Data Source	Main Processing Method
NDVI	USGS Landsat Collection 2 Level-2 Surface Reflectance	30 m	United States Geological Survey (USGS)	Calculated from red and near-infrared bands after image preprocessing.
FVC	USGS Landsat Collection 2 Level-2 Surface Reflectance	30 m	United States Geological Survey (USGS)	Derived from NDVI using the dimidiate pixel model.
Annual precipitation	China 1 km monthly precipitation dataset	1 km	National Earth System Science Data Center	Monthly precipitation data were summed to obtain annual precipitation.
Annual mean temperature	China 1 km monthly temperature dataset	1 km	National Earth System Science Data Center	Monthly mean temperature data were averaged to obtain annual mean temperature.
Riparian elevation	SRTM DEM	90 m	Resource and Environment Science and Data Center, Chinese Academy of Sciences	Extracted within the riparian buffer zone.
Riparian slope	SRTM DEM	90 m	Resource and Environment Science and Data Center, Chinese Academy of Sciences	Derived from DEM and extracted within the riparian buffer zone.
Riparian aspect	SRTM DEM	90 m	Resource and Environment Science and Data Center, Chinese Academy of Sciences	Derived from DEM and extracted within the riparian buffer zone.
Water area ratio	China Land Cover Dataset (CLCD) annual land-cover product	30 m	China Land Cover Dataset (CLCD)	Water class was extracted, and its area proportion within the riparian buffer zone was calculated.
Riparian cropland ratio	China Land Cover Dataset (CLCD) annual land-cover product	30 m	China Land Cover Dataset (CLCD)	Cropland class was extracted, and its area proportion within the riparian buffer zone was calculated.
Riparian construction-land ratio	China Land Cover Dataset (CLCD) annual land-cover product	30 m	China Land Cover Dataset (CLCD)	Construction-land class was extracted, and its area proportion within the riparian buffer zone was calculated.
Impervious-surface ratio	China Land Cover Dataset (CLCD) annual land-cover product	30 m	China Land Cover Dataset (CLCD)	Impervious-surface or built-up-land information was extracted and calculated as a proportion of the riparian buffer zone.

Table 1. *Cont.*

Indicator	Dataset	Spatial Resolution/ Statistical Unit	Data Source	Main Processing Method
Landscape fragmentation	China Land Cover Dataset (CLCD) annual land-cover product	30 m	China Land Cover Dataset (CLCD)	Landscape fragmentation was calculated based on land-use patches within the riparian buffer zone.
Riparian population density	LandScan Global Annual Population Database	30 arc-second	Oak Ridge National Laboratory (ORNL)	Mean population density was extracted within the riparian buffer zone.
Annual mean runoff	Sichuan Water Resources Bulletin, Meishan Water Resources Bulletin, and related hydrological statistics	River-section statistics	Sichuan and Meishan water resources authorities	Runoff data were matched to assessment units according to river-section location, hydrological connection, and river-system attribution.
pH	Lin et al. dataset [18] (2011, 2018); 2024 scenario-constrained regional background	Leshan Minjiangdajiao Station (MonitoringLocationIdentifier = 49)	Lin et al. dataset [18]. 2024 regional context: July 2024 Meishan Surface-Water Quality Monthly Report [19]. Additional regional context: 2024 Meishan Ecological Environment Status Bulletin [20].	2011/2018: annual station means used as common year-specific regional background values. 2024: scenario-constrained background estimates based on the monitored 2018 baseline, not direct reach-scale measurements.
NH_3-N	Lin et al. dataset [18] (2011, 2018); 2024 scenario-constrained regional background	Leshan Minjiangdajiao Station (MonitoringLocationIdentifier = 49)	Lin et al. dataset [18]. 2024 regional context: July 2024 Meishan Surface-Water Quality Monthly Report [19]. Additional regional context: 2024 Meishan Ecological Environment Status Bulletin [20].	2011/2018: annual station means used as common year-specific regional background values. 2024: scenario-constrained background estimates based on the monitored 2018 baseline, not direct reach-scale measurements.
CODMn	Lin et al. dataset [18] (2011, 2018); 2024 scenario-constrained regional background	Leshan Minjiangdajiao Station (MonitoringLocationIdentifier = 49)	Lin et al. dataset [18]. 2024 regional context: July 2024 Meishan Surface-Water Quality Monthly Report [19]. Additional regional context: 2024 Meishan Ecological Environment Status Bulletin [20].	2011/2018: annual station means used as common year-specific regional background values. 2024: scenario-constrained background estimates based on the monitored 2018 baseline, not direct reach-scale measurements.
DO	Lin et al. dataset [18] (2011, 2018); 2024 scenario-constrained regional background	Leshan Minjiangdajiao Station (MonitoringLocationIdentifier = 49)	Lin et al. dataset [18]. 2024 regional context: July 2024 Meishan Surface-Water Quality Monthly Report [19]. Additional regional context: 2024 Meishan Ecological Environment Status Bulletin [20].	2011/2018: annual station means used as common year-specific regional background values. 2024: scenario-constrained background estimates based on the monitored 2018 baseline, not direct reach-scale measurements.

2.3. Establishment of Evaluation Indicators

In accordance with the natural conditions of the Yuejiang River small watershed, data availability, and the requirements of ecological health assessment for rural rivers, this study constructed a river ecological-health-evaluation indicator system for six aspects: habitat condition, climate–hydrology, geomorphic background, water-environment condition, human-disturbance pressure, and water-quality condition. This multidimensional organization is consistent with comprehensive river-health indicator systems used in recent studies [21] (Table 2).

Table 2. Ecological health-evaluation indicator system and standardization direction for the Yuejiang River Basin.

Target Layer	Criterion Layer	Indicator	Unit	Standardization Direction
Ecological health assessment of the basin	Habitat condition B1	Riparian vegetation coverage C1	%	Positive (+)
Ecological health assessment of the basin	Habitat condition B1	Riparian vegetation condition C2	—	Positive (+)
Ecological health assessment of the basin	Habitat condition B1	Landscape fragmentation C3	patches/ km^2	Negative (−)
Ecological health assessment of the basin	Climate-driving factors B2	Annual mean temperature C4	°C	Negative (−)
Ecological health assessment of the basin	Climate-driving factors B2	Annual precipitation C5	mm	Positive (+)
Ecological health assessment of the basin	Climate-driving factors B2	Annual mean runoff C6	m^3/s	Positive (+)
Ecological health assessment of the basin	Topographic constraint B3	Riparian slope C7	°	—
Ecological health assessment of the basin	Topographic constraint B3	Riparian aspect C8	°	—
Ecological health assessment of the basin	Topographic constraint B3	Riparian elevation C9	m	—
Ecological health assessment of the basin	Water-environment condition B4	Water area ratio C10	%	Positive (+)
Ecological health assessment of the basin	Human-disturbance pressure B5	Riparian population density C11	persons/ km^2	Negative (−)
Ecological health assessment of the basin	Human-disturbance pressure B5	Riparian cropland ratio C12	%	Negative (−)
Ecological health assessment of the basin	Human-disturbance pressure B5	Riparian construction-land ratio C13	%	Negative (−)
Ecological health assessment of the basin	Human-disturbance pressure B5	Impervious-surface ratio C14	%	Negative (−)
Ecological health assessment of the basin	Water-quality condition B6	pH suitability C15	—	Positive (+)
Ecological health assessment of the basin	Water-quality condition B6	NH_3-N C16	mg/L	Negative (−)
Ecological health assessment of the basin	Water-quality condition B6	CODMn C17	mg/L	Negative (−)
Ecological health assessment of the basin	Water-quality condition B6	DO C18	mg/L	Positive (+)

Note: "+" denotes a positive indicator, "−" denotes a negative indicator, and "—" indicates that no monotonic standardization direction was assigned.

The initial indicator system comprised 18 candidate variables. Habitat condition (B1) included FVC, NDVI, and landscape fragmentation, representing riparian vegetation coverage, vegetation condition, and habitat continuity, respectively. Climate–hydrology (B2) included annual mean temperature, annual precipitation, and annual mean runoff, describing thermal background, water supply, and hydrological conditions. Geomorphic background (B3) included elevation, slope, and aspect, while water-environment condition (B4) was represented by the water-area ratio.

Human-disturbance pressure (B5) comprised riparian population density, riparian cropland ratio, riparian construction-land ratio, and impervious-surface ratio, representing population pressure, agricultural use, construction development, and surface hardening. Water-quality condition (B6) included pH, NH_3-N, CODMn, and DO, representing acid–base suitability, ammonia–nitrogen pressure, organic-pollution pressure, and oxygen conditions, respectively.

Together, these variables describe the Yuejiang River from the perspectives of natural background, ecological condition, and human disturbance. Subsequent checks of variability and correlation were used to screen the candidate set before weighting. Riparian slope, aspect, elevation, and riparian construction-land ratio showed insufficient variability for the final statistical analysis and were excluded, leaving 14 effective indicators for PCA–entropy weighting and RHI calculation.

Indicator direction was defined for the environmental range observed in the Yuejiang River, and should not be interpreted as a universal monotonic ecological relationship. FVC, NDVI, annual precipitation, annual mean runoff, water-area ratio, and DO were treated as positive indicators, whereas landscape fragmentation, riparian population density, cropland ratio, construction-land ratio, impervious-surface ratio, NH_3-N, and CODMn were treated as negative indicators. Annual mean temperature was treated as a pressure indicator within the relatively narrow local thermal range; this does not imply that higher temperature is universally detrimental. Likewise, the positive directions assigned to precipitation and runoff apply only to the observed range, and do not imply that extreme rainfall or excessive runoff is beneficial. For pH, the positive direction refers to the near-neutral suitability represented in the processed pH indicator, rather than to an assumption that a higher raw pH is always better. Elevation, slope, and aspect were included initially only to characterize geomorphic background; because their ecological effects are context-dependent and they showed little variation among assessment units, no monotonic direction was assigned, and they were excluded from the final PCA and weighting calculation.

2.4. Data Standardization and Statistical Tests

Because the indicators differed substantially in units and magnitude, direct integration of their raw values was inappropriate. Range standardization was therefore applied to transform the retained variables to the [0, 1] interval before PCA and entropy weighting, thereby removing dimensional effects while preserving relative differences among observations.

Considering the directional differences in the effects of different indicators on river ecological health, positive and negative indicators were standardized separately, following the general normalization logic used in entropy-based water-environment assessment [22]. For positive indicators, higher standardized values indicate more favorable conditions within the observed study range, and Equation (1) was used:

$$X_{ij}' = \frac{X_{ij} - min(X_j)}{max(X_j) - min(X_j)} \tag{1}$$

For negative indicators, higher raw values indicate greater ecological pressure. The direction-adjusted treatment is also consistent with recent improvements to entropy-based water-quality evaluation [23]; Equation (2) was used:

$$X_{ij}{}' = \frac{max(X_j) - X_{ij}}{max(X_j) - min(X_j)} \tag{2}$$

where $X_{ij}{}'$ is the standardized value of indicator j for assessment observation i, X_{ij} is the original value, and $max(X_j)$ and $min(X_j)$ are the maximum and minimum values of indicator j. To preserve temporal comparability, $max(X_j)$ and $min(X_j)$ were calculated from the pooled set of all 18 unit–year observations from 2011, 2018, and 2024, rather than separately for each year. An indicator with no variation across the pooled observations was excluded from the weighting calculation because it provided no discriminatory information.

2.5. Traditional Entropy Weight Method

To compare the differences in indicator weights before and after the introduction of PCA, the traditional direct entropy weight method was used as the benchmark model. The benchmark model directly calculates information entropy, the divergence coefficient, and indicator weights based on standardized indicators, without dimensionality reduction or integration of correlated indicators. Therefore, its results mainly reflect the weighting pattern determined by the degree of indicator dispersion.

First, the proportion of indicator j for assessment observation i was calculated using Equation (3):

$$P_{ij} = \frac{X'_{ij}}{\sum_{i=1}^{n} X'_{ij}} \tag{3}$$

The information entropy, divergence coefficient, and traditional entropy weight of indicator j were then calculated using Equations (4)–(6):

$$e_j = -k\sum_{i=1}^{n} P_{ij} ln(P_{ij}), \;\; k = \frac{1}{lnn} \tag{4}$$

$$d_j = 1 - e_j \tag{5}$$

$$W_{E,j} = \frac{d_j}{\sum_{j=1}^{m} d_j} \tag{6}$$

Entropy weighting provides an objective measure of information dispersion, but direct application can repeatedly count overlapping information when indicators are strongly correlated, as observed for FVC and NDVI, the water-quality variables, and several human-disturbance indicators in this study.

2.6. Principal Component Analysis and PCA–Entropy-Based Combined Weights

After standardization and correlation diagnosis, PCA was applied as an exploratory auxiliary procedure to identify common variation among correlated indicators. The analysis used an 18 × 14 matrix: 18 rows represented the six spatial assessment units for each of the three assessment years, and 14 columns represented the effective standardized indicators retained after screening. Given the limited observation-to-variable ratio, PCA was not treated as an independent evaluation model or as evidence of causal relationships; it was used only to diagnose shared information and reduce repeated representation in the weighting procedure.

The retained principal components were determined using eigenvalues greater than 1, together with the cumulative variance contribution rate. Varimax orthogonal rotation was then applied to improve interpretability. For interpretation of the rotated structure in the revised manuscript, indicators with an absolute rotated loading of ∣loading∣ ≥ 0.60 were treated as high-loading indicators for interpretation. The complete Varimax-rotated loading matrix is provided in Supplementary Table S1. The PCA contribution weight of indicator j was calculated from the absolute rotated loadings and the corresponding variance contribution rates using Equation (7):

$$W_{\mathrm{PCA},j} = \frac{\sum_{k=1}^{r} \left| a_{jk} \right| V_k}{\sum_{j=1}^{m} \sum_{k=1}^{r} \left| a_{jk} \right| V_k} \tag{7}$$

where a_{jk} is the rotated loading of indicator j on principal component k, V_k is the variance contribution rate of component k, r is the number of retained principal components, and m is the number of effective indicators. The PCA–entropy combined weight was then obtained by product normalization using Equation (8):

$$W_j = \frac{W_{\mathrm{PCA},j} W_{\mathrm{E},j}}{\sum_{j=1}^{m} W_{\mathrm{PCA},j} W_{\mathrm{E},j}} \tag{8}$$

where $W_{\mathrm{PCA},j}$ is the PCA contribution weight, $W_{\mathrm{E},j}$ is the traditional entropy weight, and W_j is the final combined weight of indicator j. All RHI values in this study were calculated using W_j.

2.7. River Health Index Construction and Health Grade Classification

Based on the PCA–entropy combined weights, the River Health Index (RHI) of the Yuejiang River was constructed as follows:

$$RHI_i = \sum_{j=1}^{m} W_j {x'}_{ij} \tag{9}$$

The RHI ranges from 0 to 1, with larger values indicating better ecological health. The normalized scale was divided a priori into five equal-width grades—Very Poor, Poor, Moderate, Good, and Excellent—to provide a consistent descriptive classification across the three assessment years. The ecological descriptions in Table 3 were formulated to match the indicator system and local environmental context.

2.8. Ecological Consistency Check Based on Land-Use Data

To examine whether the RHI results were ecologically consistent with broader environmental change, an auxiliary comparison with land-use structure was conducted. Because water-area ratio, cropland ratio, impervious-surface ratio, and landscape fragmentation were already included in the RHI calculation, land use was not treated as an independent external validation dataset. Instead, changes in forest and grassland, cropland, and construction land were used only as a contextual ecological consistency check.

Specifically, the proportions of forest and grassland, cropland, and construction land were compared with relative-RHI spatial classes derived from the descriptive spatial classification used in the RHI mapping. The two upper relative classes were aggregated as "high + relatively high" and the two lower relative classes as "low + relatively low"; the intermediate class was not included in either aggregate. These relative spatial classes were used only to summarize the distribution of RHI values for ecological-context comparison. They are distinct from the fixed five-level health grades defined in Section 2.7 and therefore should not be interpreted as an alternative health-grade classification.

Table 3. RHI health-grade classification used in this study.

Health Grade	RHI Score Range	Comprehensive Characteristics
Excellent	$0.80 < \text{RHI} \leq 1.00$	Riparian vegetation coverage is high, habitat structure is intact, connectivity between the water body and riparian zone is good, ecological buffering capacity is strong, and the river ecosystem is in a stable and healthy state.
Good	$0.60 < \text{RHI} \leq 0.80$	Vegetation condition is relatively good, riparian continuity is strong, river ecological structure is relatively intact, human disturbance is low, and the ecosystem has good self-maintenance capacity.
Moderate	$0.40 < \text{RHI} \leq 0.60$	Vegetation coverage and water-environment conditions are at a moderate level. Some river sections are affected by agricultural activities, construction land, or riparian disturbance, and ecosystem stability is moderate.
Poor	$0.20 < \text{RHI} \leq 0.40$	Riparian vegetation coverage is insufficient, river buffering capacity is weak, local habitat degradation is evident, human disturbance is strong, and ecosystem health is relatively low.
Very Poor	$0 \leq \text{RHI} \leq 0.20$	Habitat degradation is severe, vegetation is sparse, water-environment pressure is high, riparian ecological functions are seriously impaired, and ecological restoration demand is high.

Note: The five numerical intervals are equal-width classes on the normalized 0–1 RHI scale and were defined a priori for consistent comparison among assessment years. They are descriptive health grades used in this study, rather than thresholds derived from an external regulatory standard.

3. Results

3.1. Indicator Correlation and Exploratory Use of PCA

All retained indicators were standardized, as described in Section 2.4, and their dispersion was examined before PCA. Riparian slope, aspect, riparian construction land, and elevation showed limited variation among the assessment units and therefore contributed little discriminatory information for correlation diagnosis or weighting. These four variables were excluded from PCA and the final weighting calculation, although the geomorphic variables and construction-land context were retained for descriptive interpretation.

Finally, 14 effective indicators were selected for calculation, and the correlation coefficient matrix was obtained (Figure 3). As shown in the figure, the correlation coefficients among several variables exceeded 0.7. The correlation coefficients between pH and NH_3-N, and between pH and CODMn, were both 0.95. Human-disturbance and landscape-structure indicators also showed strong correlations. The correlation coefficient between riparian population density and landscape fragmentation was 0.75, while that between riparian cropland ratio and landscape fragmentation was 0.86, indicating a close relationship between human activities and riparian habitat fragmentation. Imperv was strongly positively correlated with FVC, NDVI, annual mean temperature, and DO, suggesting obvious common variation among impervious-surface change, vegetation, water quality, and landscape-structure indicators.

https://doi.org/10.3390/su18178994

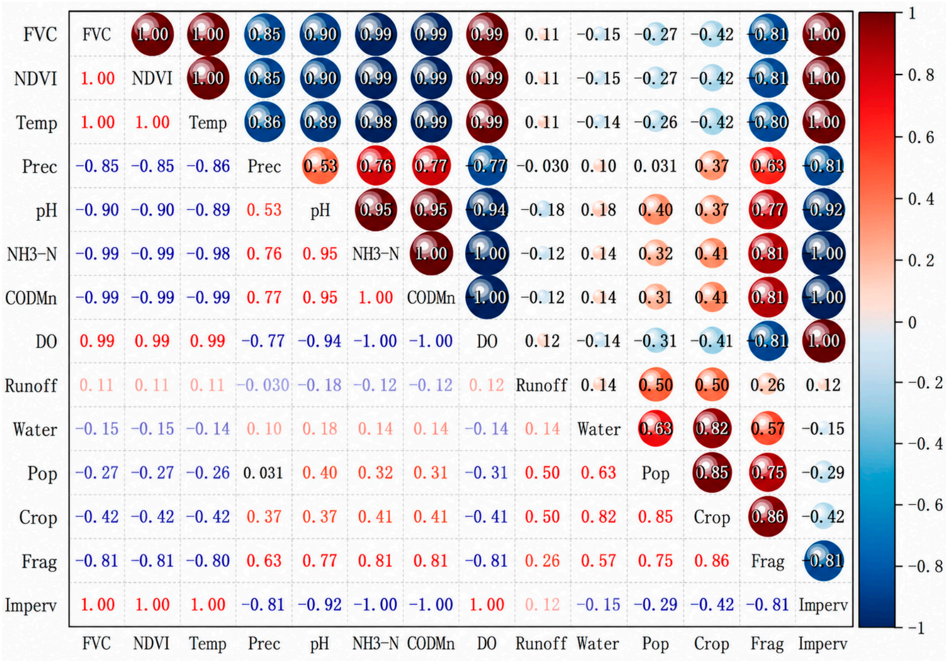

Figure 3. Pearson correlation heatmap of the 14 effective indicators. Red and blue indicate positive and negative correlations, respectively; circle size and color intensity increase with the absolute magnitude of the correlation coefficient.

These correlations indicate substantial shared information among several indicators and provide the empirical rationale for using PCA as an exploratory redundancy-diagnosis step. They should not, however, be interpreted as evidence of strong sampling adequacy for inferential PCA.

Based on the correlation analysis, KMO and Bartlett's test of sphericity were examined to assess the suitability of exploratory PCA (Table 4). The KMO value was 0.582, indicating marginal sampling adequacy and only the minimum acceptable level for exploratory use. Bartlett's test was significant (χ^2 = 2209.784, df = 91, p < 0.001), indicating that the correlation matrix differed significantly from an identity matrix. Given the limited 18 × 14 observation-to-variable structure, PCA was therefore used cautiously as an auxiliary exploratory procedure, rather than as evidence of strong statistical adequacy.

Table 4. KMO and Bartlett's test of sphericity results for the indicators.

Test Item	Statistic	df	*p*-Value	Interpretation
Kaiser–Meyer–Olkin measure of sampling adequacy	0.582	N/A	N/A	KMO = 0.582 indicates marginal sampling adequacy and only the minimum reference level for exploratory PCA.
Bartlett's test of sphericity	2209.784	91	<0.001	Bartlett's test is significant; PCA is therefore used cautiously as an exploratory auxiliary procedure.

The first four principal components were retained because each had an eigenvalue greater than 1 and the scree curve flattened after PC4 (Figure 4). These components were subsequently used to interpret the rotated loading structure and to calculate PCA contribution weights.

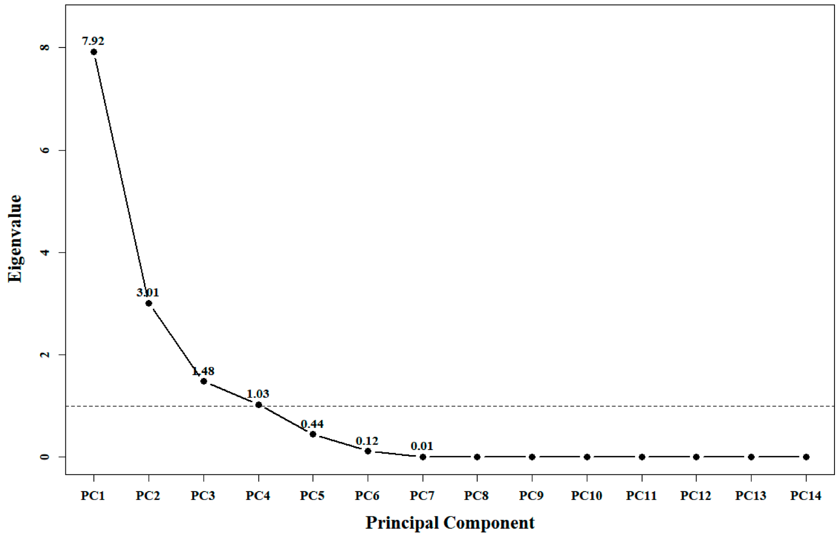

Figure 4. Scree plot of principal component analysis. The dashed horizontal line marks the eigenvalue = 1 retention criterion.

3.2. Principal Component Extraction and Ecological Implications

Principal component extraction was performed on the standardized matrix of the 14 effective indicators. Using the eigenvalue-greater-than-one criterion, four components were retained, together explaining 95.94% of the total variance (Table 5). This high cumulative proportion indicates that the retained components captured most of the variance contained in the screened indicator set.

Table 5. Eigenvalues and variance contribution rates before and after rotation.

Main Component	Before Rotation			After Rotation		
	Eigenvalue	Variance Contribution Rate (%)	Accumulated Contribution Rate (%)	Eigenvalue	Variance Contribution Rate (%)	Accumulated Contribution Rate (%)
PC1	7.919	56.56	56.56	7.698	54.99	54.99
PC2	3.007	21.48	78.05	2.896	20.69	75.67
PC3	1.477	10.55	88.59	1.580	11.29	86.96
PC4	1.028	7.34	95.94	1.257	8.98	95.94

Before rotation, PC1 and PC2 explained 56.56% and 21.48% of the total variance, respectively, for a cumulative contribution of 78.05%; PC1–PC4 together explained 95.94%. Figure 5 displays the 18 unit–year observations and the loading directions of the 14 effective indicators in the PC1–PC2 space. The biplot is used only to support interpretation of relationships among indicators and observations. Because Figure 5 is based on unrotated components, ecological interpretation of the four retained components is based on the Varimax-rotated loading structure. In the PC1–PC2 ordination, the 18 unit–year observations show a clear temporal separation along PC1: the 2011 observations are located mainly on the negative side, the 2024 observations on the positive side, and the 2018 observations occupy an intermediate position. This pattern indicates that PC1 mainly captures a broad temporal gradient in the multivariate indicator set. FVC and NDVI point in similar directions, consistent with their close relationship in Figure 3, while several other indicators form distinct directional groups in the ordination space. These vector relationships describe covariance in the first two unrotated components, and are not interpreted as direct ecological effects or causal relationships.

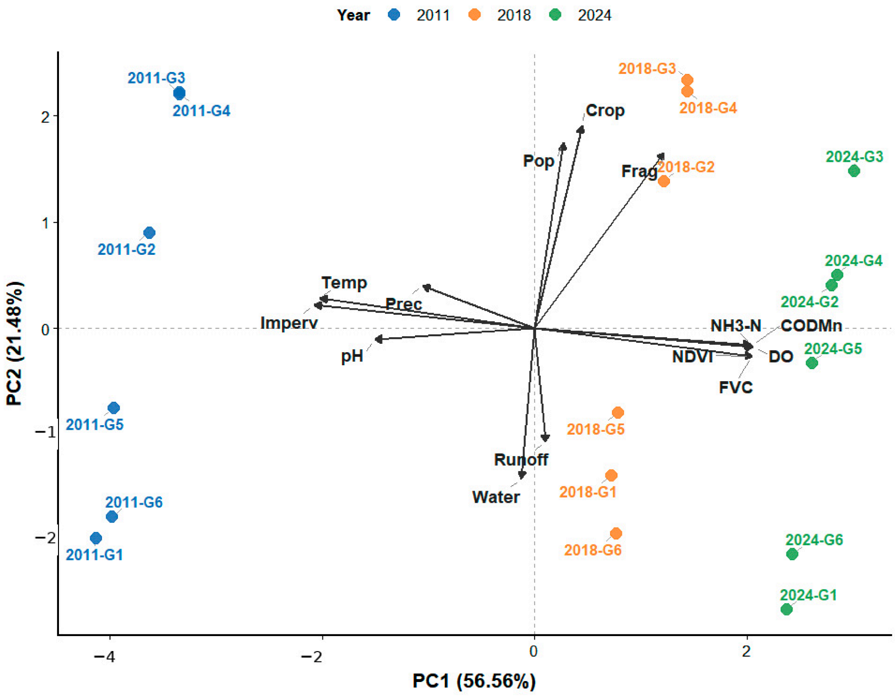

Figure 5. PCA biplot of the 14 ecological health indicators. Negative axis values are shown with the mathematical minus sign (−).

Varimax rotation produced a clearer loading structure, allowing the retained components to be interpreted in terms of common variation among vegetation, water quality, hydroclimatic conditions, landscape structure, and human disturbance.

Using an absolute rotated-loading threshold of $|\text{loading}| \geq 0.60$, PC1 showed high loadings for FVC, NDVI, annual mean temperature, pH, NH_3-N, CODMn, DO, and Imperv (Supplementary Table S1). PC1 therefore represents a broad pattern of common temporal variation involving riparian vegetation, water-quality variables, thermal background, and impervious-surface conditions. Because PCA loadings describe covariance rather than causation, this component is interpreted as a shared statistical pattern rather than as evidence that any individual indicator directly controlled river health.

PC2 showed high absolute loadings for Water, Pop, Crop, and Frag, reflecting variation in water-space conditions, riparian landscape structure, and human disturbance among assessment units. PC3 was dominated by annual precipitation, whereas PC4 was dominated by annual mean runoff (Table 6). Secondary cross-loadings shown in Supplementary Table S1 were retained in the PCA contribution-weight calculation through their absolute values, but were not used to assign additional dominant indicators below the stated interpretation threshold.

Table 6. Main high-loading indicators of the rotated principal components.

Component	Main High-Loading Indicators	Ecological Implication
PC1	FVC, NDVI, Temp, pH, NH_3-N, CODMn, DO, Imperv	Common temporal variation in vegetation, water quality, thermal background, and impervious-surface conditions
PC2	Water, Pop, Crop, Frag	Water-space contrast, riparian landscape structure, and human disturbance
PC3	Prec	Precipitation-related hydroclimatic variation
PC4	Runoff	Runoff variation among assessment units

3.3. Entropy Weights and Comparison Between Traditional and Improved Weighting Methods

To evaluate how PCA altered the weight structure, PCA contribution weights, traditional entropy weights, and final combined weights were calculated for the 14 effective indicators (Table 7). Traditional entropy weights primarily reflect the dispersion of each indicator. Water-area ratio and annual mean runoff therefore received relatively high entropy weights (0.143203 and 0.140688, respectively), indicating substantial variation among assessment units. Such dispersion, however, should not be interpreted as evidence of ecological dominance.

Table 7. PCA weights, entropy weights, and combined weights of the 14 indicators.

Indicator	PCA Contribution Weight	Entropy Weight	Combined Weight	Rank
FVC	0.0918	0.0660	0.0888	4
NDVI	0.0918	0.0660	0.0888	3
Temp	0.0912	0.0722	0.0965	2
Prec	0.0541	0.0627	0.0496	11
pH	0.0843	0.0718	0.0887	5
NH_3-N	0.0908	0.0613	0.0816	7
CODMn	0.0903	0.0615	0.0814	8
DO	0.0900	0.0616	0.0812	9
Runoff	0.0306	0.1407	0.0631	10
Water	0.0419	0.1432	0.0879	6
Pop	0.0401	0.0416	0.0244	13
Crop	0.0397	0.0350	0.0204	14
Frag	0.0714	0.0295	0.0308	12
Imperv	0.0919	0.0868	0.1168	1

Incorporating PCA redistributed the weight structure. The combined weights of annual mean runoff and water-area ratio decreased to 0.063109 and 0.087907, respectively, indicating that the combined procedure reduced the relative influence of indicators that were highly dispersed when considered independently. Imperv, annual mean temperature, NDVI, FVC, pH, NH_3-N, CODMn, and DO retained comparatively high combined weights. Imperv had the largest combined weight (0.116823), whereas NDVI and FVC had weights of 0.088774 and 0.088751. These values indicate statistical contributions to RHI variation within the present framework, and should not be interpreted as evidence of direct ecological causation.

The combined weight of annual mean temperature was 0.096479. This value reflects its statistical contribution within the weighting framework and the temporal thermal background represented by the indicator; it does not imply that temperature was an independent or decisive ecological driver. Overall, PCA–entropy weighting retained information on indicator dispersion while moderating the relative influence of some highly dispersed or correlated variables.

3.4. Statistical Characteristics and Temporal Variation in the RHI

RHI values for 2011, 2018, and 2024 were calculated using the PCA–entropy combined weights. Mean RHI increased from 0.290 in 2011 (Grade IV, Poor) to 0.578 in 2018 (Grade III, Moderate) and 0.634 in 2024 (Grade II, Good) (Figure 6). These values represent differences among three discrete assessment years, rather than a continuous annual trajectory.

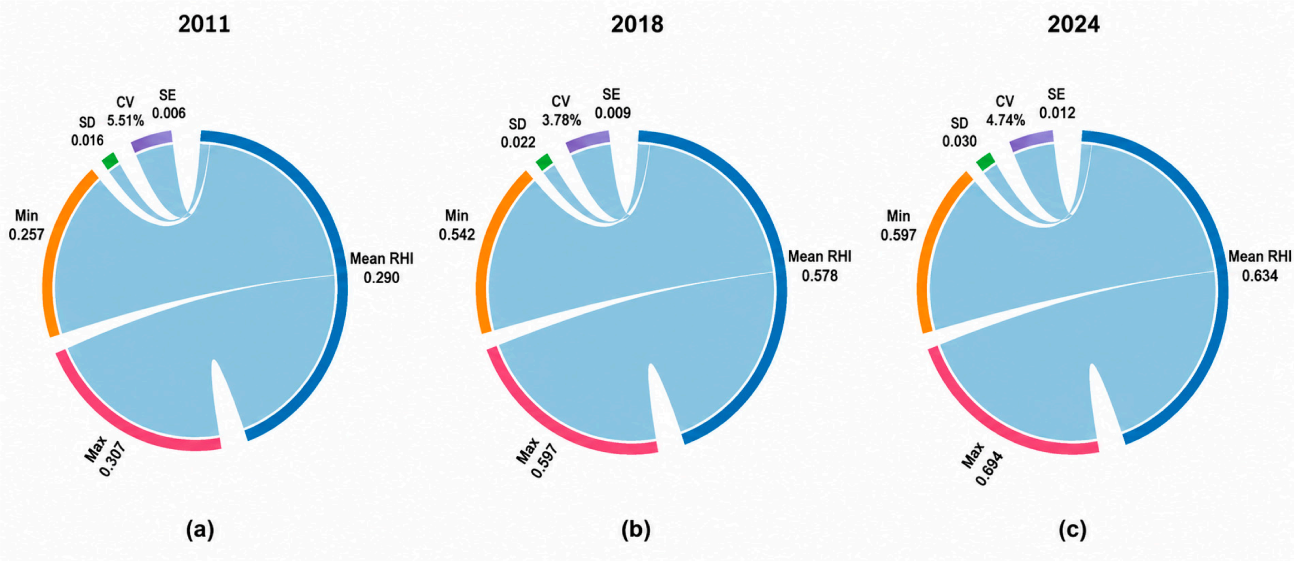

Figure 6. Chord diagrams showing the statistical characteristics of RHI in 2011 (**a**), 2018 (**b**), and 2024 (**c**). Colors distinguish the mean RHI, minimum, maximum, standard deviation (SD), coefficient of variation (CV), and standard error (SE).

RHI ranged from 0.257 to 0.307 in 2011, and all assessment units fell within the Poor grade, indicating generally weak ecological condition at the beginning of the study period. In 2018, values increased to 0.542–0.597 and all units were classified as Moderate. By 2024, RHI ranged from 0.597 to 0.694 and most units had entered the Good grade; however, the minimum value remained close to the 0.60 boundary between Moderate and Good, indicating persistent local weakness.

The standard deviations of RHI were 0.020, 0.020, and 0.032 in 2011, 2018, and 2024, respectively, with corresponding coefficients of variation of 0.068, 0.035, and 0.051. The lowest coefficient of variation occurred in 2018, indicating relatively small differences among units. In 2024, the higher mean RHI was accompanied by greater spatial dispersion. Because the 2024 water-quality inputs are scenario-constrained regional background estimates rather than direct measurements for the six units, the 2024 RHI statistics should be interpreted as conditional composite-assessment results, rather than as measured reach-scale water-quality outcomes.

3.5. Changes in River Health Grades

The health-grade structure also changed across the three assessment years (Table 8). In 2011, the mapped assessment area was entirely classified as Grade IV (Poor). In 2018, it was entirely Grade III (Moderate), indicating an overall improvement but not yet an attainment of the Good grade.

Table 8. Changes in RHI grades and mapped-area proportions.

Year	Grade V: Very Poor/%	Grade IV: Poor/%	Grade III: Moderate/%	Grade II: Good/%	Grade I: Excellent/%	Grade III and Below/%	Grade II and Above/%	Dominant Health Grade
2011	0.00	100.00	0.00	0.00	0.00	100.00	0.00	Grade IV: Poor
2018	0.00	0.00	100.00	0.00	0.00	100.00	0.00	Grade III: Moderate
2024	0.00	0.00	16.08	83.92	0.00	16.08	83.92	Grade II: Good

By 2024, 83.92% of the mapped assessment area was classified as Grade II (Good) and 16.08% as Grade III (Moderate), indicating that most of the assessed area had reached a comparatively good condition. Local weakness, nevertheless, remained, consistent with the minimum RHI value of 0.597. These 2024 mapped-area proportions are conditional on the adopted water-quality background scenario, and should be interpreted together with the uncertainty discussed in Section 4.4.

The percentages in Table 8 are mapped-area proportions, not counts of the six assessment units. At the assessment-unit level (Figure 7), all six units were Poor in 2011 and Moderate in 2018. In 2024, five units reached Grade II (Good), whereas the middle tributary remained Grade III (Moderate) with an RHI of 0.597, close to the 0.60 threshold for Good. This reach was therefore identified as the relatively weakest unit in 2024.

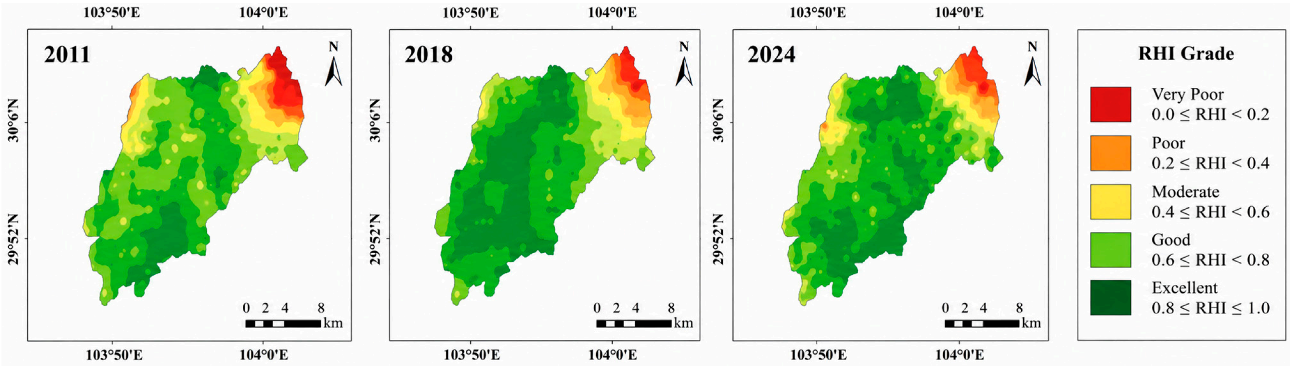

Figure 7. Spatial distribution of RHI in 2011, 2018, and 2024.

Considering the spatial pattern together with the weighting results, the relatively weak condition of the middle tributary is consistent with its proximity to riparian cropland, human disturbance, and local water-environment pressure. This interpretation is associative rather than causal, and supports prioritizing the reach for riparian restoration and water-environment management.

3.6. Rationality Check of RHI Results and Ecological Consistency Analysis Based on Land Use

To examine ecological consistency, the spatial RHI pattern was compared with land-use change between 2011 and 2024. Cropland remained the dominant land-use type, forest was concentrated mainly in the northeastern basin and local riparian areas, construction land occurred in scattered patches, and water bodies followed the main channel and tributaries (Figure 8). This comparison is used only as contextual support, and not as independent external validation.

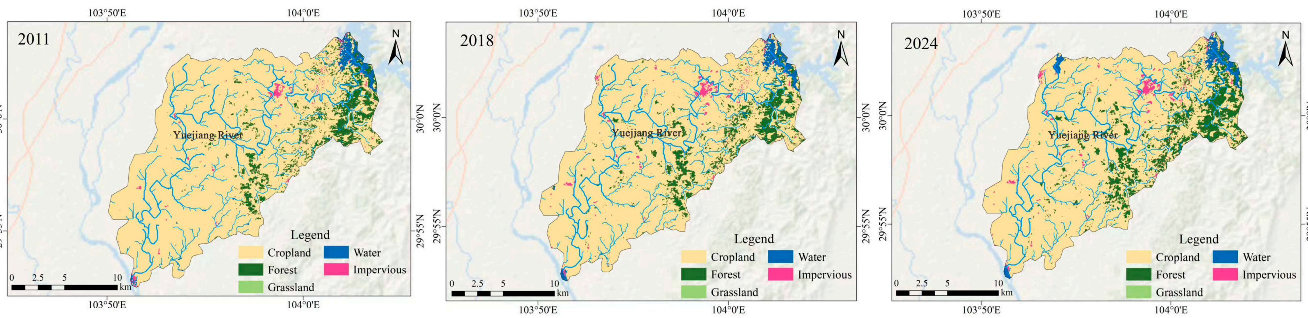

Figure 8. Spatial distribution of land-use types in the Yuejiang River Basin in 2011, 2018, and 2024.

From 2011 to 2024, the combined proportion of forest and grassland increased from 0.82% to 1.98%, while the combined proportion of high and relatively high relative-RHI spatial classes increased from 4.71% to 14.02%. Cropland and construction land remained dominant, alongside a large share of low and relatively low relative-RHI classes. The parallel changes provide qualitative ecological consistency between RHI patterns and land-use structure, but they do not constitute independent validation because several land-use-related variables were already included in the RHI calculation (Table 9).

Table 9. Ecological consistency check between relative-RHI spatial classes and land-use structure in the Yuejiang River Basin.

Year	High + Relatively High Relative-RHI Spatial Classes/%	Low + Relatively Low Relative-RHI Spatial Classes/%	Forest + Grassland/%	Cropland + Construction Land/%
2011	4.71	73.33	0.82	97.75
2018	4.43	80.65	1.94	96.72
2024	14.02	66.94	1.98	96.89

Note: The relative-RHI classes in Table 9 are descriptive spatial categories used only for contextual comparison with land-use structure. They are not the fixed RHI health grades defined in Table 3 and should not be interpreted as an independent validation or an alternative health classification.

4. Discussion

4.1. Applicability of the Indicator System

Water-quality indices are useful for describing pollution status, but do not capture the full ecological condition of a river [24–29]. River-health studies therefore increasingly combine water quality with habitat, hydrology, landscape structure, and human disturbance [30,31]. Studies of urban rivers, riverine wetlands, estuaries, and mixed land-use watersheds [32,33] also report marked spatial heterogeneity. The Yuejiang River shows a similar pattern: most units reached the Good grade in 2024, whereas the middle tributary remained Moderate. This comparison is qualitative because indicator systems differ among studies and long-term aquatic biological data were unavailable here.

For a small rural watershed, the main value of the present indicator system is that riparian vegetation, hydrological conditions [34,35], regional water-quality background, landscape structure, and human disturbance are considered together. This supports temporal comparison and identification of local weak reaches, but it does not replace direct biological or reach-scale water-quality monitoring.

4.2. Effects of the PCA–Entropy Method on Weighting Results

Entropy weighting reflects indicator dispersion but does not remove overlapping information among correlated variables. In the Yuejiang River dataset, FVC and NDVI, the four water-quality variables, and several human-disturbance indicators showed clear shared variation. PCA was therefore introduced as an exploratory step to diagnose this covariance before combined weighting.

Four retained components explained 95.94% of the total variance. At $|\text{loading}| \geq 0.60$, PC1 represented common variation in FVC, NDVI, Temp, pH, NH_3-N, CODMn, DO, and Imperv; PC2 represented Water, Pop, Crop, and Frag; PC3 was associated mainly with Prec; and PC4 with Runoff. These groupings describe statistical covariance, and should not be interpreted as causal pathways.

Water and Runoff had relatively high entropy weights (0.143203 and 0.140688), but their combined weights decreased to 0.087907 and 0.063109 after PCA information was incorporated. Imperv and several vegetation and water-quality indicators retained relatively high combined weights. This redistribution illustrates how the combined procedure balances dispersion and covariance; it does not demonstrate direct ecological causation.

4.3. RHI Changes and Identification of Weak River Sections

Across the three assessment years, mean RHI increased from 0.290 to 0.578 and 0.634. In 2024, 83.92% of the mapped assessment area was Good and 16.08% was Moderate; at the assessment-unit level, five of the six units were Good, while the middle tributary remained the weakest unit (RHI = 0.597). The results indicate overall improvement accompanied by persistent local differences.

Such local differences are plausible in agricultural and mixed land-use watersheds, where land use, riparian landscape structure, and non-point-source pollution are closely associated with stream condition [36–41]. Cropland and construction land remain dominant in the Yuejiang River Basin, and the middle tributary is close to these pressures. This supports prioritizing that reach for riparian and water-environment management without treating the weighting results as direct causal evidence.

Riparian studies also emphasize buffer configuration, vegetation condition, and vegetation–hydromorphology interactions in river management [42–45]. In this study, forest and grassland increased from 0.82% to 1.98%, while high and relatively high RHI areas increased from 4.71% to 14.02%. The parallel trend provides an ecological consistency check, not independent validation, because vegetation- and land-use-related indicators were already included in the RHI.

4.4. Management Implications and Limitations

Management should prioritize the middle tributary and other relatively weak reaches. Key actions include restoring riparian vegetation, reducing direct cropland–channel contact, controlling agricultural and domestic pollution inputs, and limiting additional riparian hardening. Reaches already classified as Good should be managed to maintain vegetation continuity and prevent new disturbance.

Several limitations remain. The 2011 and 2018 water-quality data represent regional background conditions from the Leshan Minjiangdajiao station, rather than reach-scale measurements [46]. For 2024, continuous observations for the six Yuejiang River units were unavailable. The July 2024 monthly report and the 2024 status bulletin described in Section 2.2 were used only as regional contextual checks, and not as direct numerical sources for individual reaches. The numerical 2024 inputs were predefined scenario-constrained regional background estimates anchored to the monitored 2018 annual background, with only limited scenario differences among mainstream/tributary and upper/middle/lower units; no reach-scale interpolation from monitoring observations was performed. The 2024 RHI should therefore be read as a conditional exploratory estimate, rather than as evidence of measured reach-scale water-quality change. In addition, the analysis uses only three assessment years, PCA is based on an 18×14 matrix, and comparable long-term aquatic biological indicators were unavailable. Future work should prioritize continuous local water-quality and biological monitoring.

5. Conclusions

(1) The 14 effective indicators contained substantial shared information. PCA retained four components explaining 95.94% of the total variance and was used as an exploratory redundancy-diagnosis step because the analysis matrix contained only 18 observations.

(2) Mean RHI values were 0.290, 0.578, and 0.634 in 2011, 2018, and 2024, respectively. In 2024, 83.92% of the mapped assessment area was Good and 16.08% was Moderate; at the assessment-unit level, five of the six units were Good, while the middle tributary remained Moderate (RHI = 0.597). The 2024 result is conditional on the adopted water-quality background scenario.

(3) PCA–entropy weighting moderated the relative influence of some highly dispersed or correlated indicators while retaining substantial weights for Imperv, vegetation, and water-quality variables. These weights represent statistical contributions within the assessment framework, rather than direct ecological causation.

(4) Management should prioritize weak reaches through riparian restoration, non-point-source pollution control, and protection of existing good-condition sections. Future assessments should incorporate continuous local water-quality monitoring, denser temporal observations, and aquatic biological indicators.

Supplementary Materials: The following supporting information can be downloaded at: https://www.mdpi.com/article/10.3390/su18178994/s1.

Author Contributions: Conceptualization, D.W. and W.C.; methodology, D.W.; software, D.W.; formal analysis, D.W.; investigation, D.W.; data curation, D.W.; writing—original draft preparation, D.W.; writing—review and editing, W.C., J.Z., R.H., Y.H. and H.X.; visualization, D.W.; supervision, W.C.; project administration, W.C.; funding acquisition, W.C. All authors have read and agreed to the published version of the manuscript.

Funding: This research was funded by the Sichuan Federation of Social Sciences, grant number SC20EZD003.

Institutional Review Board Statement: Not applicable.

Informed Consent Statement: Not applicable.

Data Availability Statement: The datasets supporting the findings of this study are described in Table 1 and the cited data sources. The exact water-quality inputs used in the analysis and the rotated PCA loading matrix are provided in the Supplementary Materials (Tables S1 and S2). Additional processed data are available from the corresponding author upon reasonable request.

Conflicts of Interest: The authors declare no conflict of interest.

References

1. Xue, C.Y.; Shao, C.F.; Chen, S.H. SDGs-Based River Health Assessment for Small- and Medium-Sized Watersheds. *Sustainability* **2020**, *12*, 1846. [CrossRef]
2. Su, Y.; Li, W.; Liu, L.; Hu, W.; Li, J.; Sun, X.; Li, Y. Health assessment of small-to-medium sized rivers: Comparison between comprehensive indicator method and biological monitoring method. *Ecol. Indic.* **2021**, *126*, 107686. [CrossRef]
3. Xu, F.; Wang, Y.G.; Wang, X.; Wu, D.; Wang, Y. Establishment and Application of the Assessment System on Ecosystem Health for Restored Urban Rivers in North China. *Int. J. Environ. Res. Public Health* **2022**, *19*, 5619. [CrossRef] [PubMed]
4. Li, J.; Huang, L.; Zhu, K. Ecological Health Assessment of an Urban River: The Case Study of Zhengzhou City, China. *Sustainability* **2023**, *15*, 8288. [CrossRef]
5. Shan, C.; Dong, Z.; Lu, D.; Xu, C.; Wang, H.; Ling, Z.; Liu, Q. Study on river health assessment based on a fuzzy matter-element extension model. *Ecol. Indic.* **2021**, *127*, 107742. [CrossRef]
6. Fu, Y.; Liu, Y.; Xu, S.; Xu, Z. Assessment of a Multifunctional River Using Fuzzy Comprehensive Evaluation Model in Xiaoqing River, Eastern China. *Int. J. Environ. Res. Public Health* **2022**, *19*, 12264. [CrossRef] [PubMed]
7. Wang, P.; Fu, Y.; Liu, P.; Zhu, B.; Wang, F.; Pamucar, D. Evaluation of ecological governance in the Yellow River basin based on Uninorm combination weight and MULTIMOORA-Borda method. *Expert Syst. Appl.* **2024**, *235*, 121227. [CrossRef]
8. Jiao, H.; Li, Y.; Wei, H.; Liu, J.; Cheng, L.; Chen, Y. Construction of River Health Assessment System in Areas with Significant Human Activity and Its Application. *Water* **2023**, *15*, 2969. [CrossRef]
9. Huang, D.; Tian, C.; Wu, W.; Shen, D.; Sang, J.; Wang, H. Comprehensive River Health Evaluation Indicator System and Its Application. *Pol. J. Environ. Stud.* **2025**, *34*, 1165–1177. [CrossRef] [PubMed]
10. Du, J.; Gao, H.; Liu, R.; Han, Y.; Hu, R. Study on assessment of water system health in Heihe River Basin based on the game theory. *Ecol. Indic.* **2025**, *174*, 113449. [CrossRef]
11. Zhang, W.; Fang, G.; Ju, M.; Cheng, T.; Zhang, S. Integrating management practices into river health assessment: A cloud model framework for small and medium rivers under uncertainty. *J. Hydrol. Reg. Stud.* **2026**, *64*, 103280. [CrossRef]
12. Chen, C.-F.; Chen, S.-K. Advancing River Health Assessment: An Integrated ISC Methodology Applied to Taiwan's River Restoration Case Study. *Sustainability* **2026**, *18*, 1007. [CrossRef]

13. Hu, Y.; Hou, X.; Men, J.; Feng, L.; Wang, T. Global evaluation revealed large spectral reflectance uncertainties in Landsat 8 Collection 2 surface reflectance products for inland and coastal waters. *ISPRS J. Photogramm. Remote Sens.* **2025**, *230*, 962–982. [CrossRef]
14. Hu, X.; Shi, S.; Zhou, B.; Ni, J. A 1 km monthly dataset of historical and future climate changes over China. *Sci. Data* **2025**, *12*, 436. [CrossRef] [PubMed]
15. Liu, S.; Wang, H.; Hu, Y.; Zhang, M.; Zhu, Y.; Wang, Z.; Li, D.; Yang, M.; Wang, F. Land Use and Land Cover Mapping in China Using Multimodal Fine-Grained Dual Network. *IEEE Trans. Geosci. Remote Sens.* **2023**, *61*, 4405219. [CrossRef]
16. Zafar, Z.; Zubair, M.; Zha, Y.; Fahd, S.; Nadeem, A.A. Performance assessment of machine learning algorithms for mapping of land use/land cover using remote sensing data. *Egypt. J. Remote Sens. Space Sci.* **2024**, *27*, 216–226. [CrossRef]
17. Lebakula, V.; Sims, K.; Reith, A.; Rose, A.; McKee, J.; Coleman, P.; Kaufman, J.; Urban, M.; Jochem, C.; Whitlock, C.; et al. LandScan Global 30 Arcsecond Annual Global Gridded Population Datasets from 2000 to 2022. *Sci. Data* **2025**, *12*, 495. [CrossRef] [PubMed]
18. Lin, J.; Wang, P.; Wang, J.; Zhou, Y.; Zhou, X.; Yang, P.; Zhang, H.; Cai, Y.; Yang, Z. An extensive spatiotemporal water quality dataset covering four decades (1980–2022) in China. *Earth Syst. Sci. Data* **2024**, *16*, 1137–1149. [CrossRef]
19. Meishan Municipal Bureau of Ecology and Environment. *2024 July Meishan Surface-Water Quality Monthly Report*; Meishan Municipal Bureau of Ecology and Environment: Meishan, China, 2024.
20. Meishan Municipal Bureau of Ecology and Environment. *2024 Meishan Ecological Environment Status Bulletin*; Meishan Municipal Bureau of Ecology and Environment: Meishan, China, 2025.
21. Shao, W.; Han, G.; Li, J.; Yang, Z.; Liu, J.; Xu, T. Establishing a river health evaluation index system for seven rivers in Jiamusi City of China. *Water Sci. Technol.* **2024**, *89*, 2254–2272. [CrossRef] [PubMed]
22. Guo, Y.; Song, Y.; Huang, J.; Zhang, L. Water Environment Assessment of Xin'an River Basin in China Based on DPSIR and Entropy Weight-TOPSIS Models. *Water* **2025**, *17*, 781. [CrossRef]
23. Yan, Q.; Yan, F.; Xie, L.; Huang, J.; Chen, R.; Liu, X. An Improved Entropy Weight Method Mitigating Grade Distortion in Water Quality Assessment. *Water* **2025**, *17*, 3508. [CrossRef]
24. Nikolaidis, N.P.; Poikane, S.; Bouraoui, F.; Salas-Herrero, F.; Free, G.; Varkitzi, I.; van de Bund, W.; Kelly, M.G. Comparison of eutrophication assessment for the Nitrates and Water Framework Directives: Impacts and opportunities for streamlined approaches. *Ecol. Indic.* **2025**, *177*, 113375. [CrossRef]
25. Nong, X.; Shao, D.; Zhong, H.; Liang, J. Evaluation of water quality in the South-to-North Water Diversion Project of China using the water quality index (WQI) method. *Water Res.* **2020**, *178*, 115781. [CrossRef] [PubMed]
26. Uddin, M.G.; Nash, S.; Rahman, A.; Olbert, A.I. A comprehensive method for improvement of water quality index (WQI) models for coastal water quality assessment. *Water Res.* **2022**, *219*, 118532. [CrossRef] [PubMed]
27. Chidiac, S.; El Najjar, P.; Ouaini, N.; El Rayess, Y.; El Azzi, D. A comprehensive review of water quality indices (WQIs): History, models, attempts and perspectives. *Rev. Environ. Sci. Bio/Technol.* **2023**, *22*, 349–395. [CrossRef] [PubMed]
28. Ding, F.; Zhang, W.; Cao, S.; Hao, S.; Chen, L.; Xie, X.; Li, W.; Jiang, M. Optimization of water quality index models using machine learning approaches. *Water Res.* **2023**, *243*, 120337. [CrossRef] [PubMed]
29. Li, X.Y.; Yan, L.; Zhi, X.; Hu, P.; Shang, C.; Zhao, B. Characteristics of the macroinvertebrate community structure and their habitat suitability conditions in the Chishui River. *Front. Ecol. Evol.* **2025**, *12*, 1459468. [CrossRef]
30. Han, H.; Li, X.; Gu, X.; Li, G. Urban rivers health assessment based on the concept of resilience using improved FCM-EWM-MABAC model. *Ecol. Indic.* **2023**, *154*, 110833. [CrossRef]
31. Dutta, A.; Karmakar, S.; Das, S.; Banerjee, M.; Ray, R.; Hasher, F.F.B.; Mishra, V.N.; Zhran, M. Modeling the River Health and Environmental Scenario of the Decaying Saraswati River, West Bengal, India, Using Advanced Remote Sensing and GIS. *Water* **2025**, *17*, 965. [CrossRef]
32. Gao, Z.; Li, C.; Zou, S.; Xie, X.; Wang, Y.; Shen, N.; Zhang, X.; Li, M. Riverine wetland dynamics and health assessment: A case study in the urban agglomerations along the Yellow River in China's Ningxia Hui Autonomous Region. *Ecol. Indic.* **2024**, *162*, 111965. [CrossRef]
33. Wang, Z.; Tian, Y.; Gong, Y.; Lan, D.; Yu, A.; Fan, P.; Yang, X.; Xu, S. Assessment of estuarine ecosystem health and its applications in the Yellow River estuary and the Yangtze River estuary. *Estuar. Coast. Shelf Sci.* **2026**, *340*, 110070. [CrossRef]
34. Feng, Y.J.; Zhu, A.K. Spatiotemporal differentiation and driving patterns of water utilization intensity in Yellow River Basin of China: Comprehensive perspective on the water quantity and quality. *J. Clean. Prod.* **2022**, *369*, 133395. [CrossRef]
35. Dai, D.; Lei, K.; Wang, R.; Lv, X.B.; Hu, J.X.; Sun, M.D. Evaluation of river restoration efforts and a sharp decrease in surface runoff for water quality improvement in North China. *Environ. Res. Lett.* **2022**, *17*, 044028. [CrossRef]
36. Lee, J.-W.; Park, S.-R.; Lee, S.-W. Effect of Land Use on Stream Water Quality and Biological Conditions in Multi-Scale Watersheds. *Water* **2023**, *15*, 4210. [CrossRef]
37. Locke, K.A. Modelling relationships between land use and water quality using statistical methods: A critical and applied review. *J. Environ. Manag.* **2024**, *362*, 121290. [CrossRef] [PubMed]

38. Cheng, C.; Zhang, F.; Shi, J.; Kung, H.-T. What is the relationship between land use and surface water quality? A review and prospects from remote sensing perspective. *Environ. Sci. Pollut. Res.* **2022**, *29*, 56887–56907. [CrossRef] [PubMed]
39. Xu, Q.; Yan, T.; Wang, C.; Hua, L.; Zhai, L. Managing landscape patterns at the riparian zone and sub-basin scale is equally important for water quality protection. *Water Res.* **2023**, *229*, 119280. [CrossRef] [PubMed]
40. Tahiru, A.A.; Doke, D.A.; Baatuuwie, B.N. Effect of land use and land cover changes on water quality in the Nawuni Catchment of the White Volta Basin, Northern Region, Ghana. *Appl. Water Sci.* **2020**, *10*, 198. [CrossRef]
41. Jones, J.; Gyawali, B.R.; Acharya, S.; Cristan, R.; Gebremedhin, M. Assessing the Influence of Agricultural Nonpoint Source Pollution on Water Quality in Central Kentucky's Headwater Streams. *Appl. Sci.* **2024**, *14*, 2679. [CrossRef]
42. Song, M.; Jiang, Y.; Liu, Q.; Tian, Y.; Liu, Y.; Xu, X.; Kang, M. Catchment versus Riparian Buffers: Which Land Use Spatial Scales Have the Greatest Ability to Explain Water Quality Changes in a Typical Temperate Watershed? *Water* **2021**, *13*, 1758. [CrossRef]
43. Duxbury, E.; Fryirs, K.; Leishman, M.R. Benchmarking Riparian Vegetation Quality in Recovering Rivers: Implications for Management of Novel Ecosystems. *Environ. Manag.* **2025**, *75*, 221–239. [CrossRef] [PubMed]
44. Rodríguez-González, P.M.; Abraham, E.; Aguiar, F.; Andreoli, A.; Baležentienė, L.; Berisha, N.; Bernez, I.; Bruen, M.; Bruno, D.; Camporeale, C.; et al. Bringing the margin to the focus: 10 challenges for riparian vegetation science and management. *WIREs Water* **2022**, *9*, e1604. [CrossRef]
45. Te Ngaio, P.A.J.; McMahon, J.M.; van den Berg, D.; Healy, A.; Turner, R.D.R.; Marsh, A. Increasing riparian vegetation cover to improve water quality: The importance of considering land use. *Environ. Manag.* **2026**, *76*, 174. [CrossRef] [PubMed]
46. Zhang, F.; Lin, L.; Li, W.; Fang, D.; Lv, Z.; Li, M.; Ma, G.; Wang, Y.; Wang, L.; He, L. Long-Term Study of Monitoring History and Change Trends in Surface Water Quality in China. *Water* **2022**, *14*, 2134. [CrossRef]